CMIP6 projections of future MJO changes under steepened moisture gradient conditions over the Indo-Pacific warm pool

Jiabao Wang*[1], Michael J. DeFlorio[1], Hyemi Kim[2,3], Kristen Guirguis[1], Alexander Gershunov[1]

[1] *Center for Western Weather and Water Extremes, Scripps Institution of Oceanography, University of California, San Diego, La Jolla, California*
[2] *Department of Science Education, Ewha Womans University, Seoul, Republic of Korea*
[3] *School of Marine and Atmospheric Sciences, Stony Brook University, Stony Brook, New York, USA*

Geophysical Research Letters

Submitted in March 2023

Key Points:

- Multi-model mean of 23 CMIP6 models projects stronger MJO convection, faster propagation speed, and an eastward extension
- Future changes in the MJO can be attributed to the steepening of the mean meridional moisture gradient over the Indo-Pacific warm pool

Corresponding author address: Jiabao Wang (jiw093@ucsd.edu)

Center for Western Weather and Water Extremes (CW3E), Scripps Institution of Oceanography, University of California, San Diego, La Jolla, CA, USA

Abstract

The Madden-Julian oscillation (MJO) has remarkable impacts on global weather and climate systems. Understanding its changes under a warming climate provides insights into how MJO-related phenomena may change accordingly. This study examines the future changes in MJO projected by 23 Coupled Model Intercomparison Project Phase 6 (CMIP6) models that produce a realistic MJO propagation in their historical runs. Results from the multi-model mean show a ~17% increase in MJO precipitation amplitude, a ~9% increase in propagation speed, a ~2-day decrease in MJO period, and a ~5° eastward extension. Analysis of the lower tropospheric moisture budget suggests the dominant role of an increased meridional advection of mean moisture caused by the steepening of mean moisture over the Indo-Pacific warm pool in a warming climate. This leads to a stronger positive moisture tendency to the east of MJO convection, and hence a more eastward MJO propagation with strengthened amplitude and faster speed.

Plain Language Summary

The Madden-Julian oscillation (MJO) is the dominant mode of intraseasonal variability in the tropics and is characterized as an eastward-propagating convection system that usually initiates in the Indian Ocean and terminates in the Pacific. As the MJO propagates, it influences weather and climate systems globally. Previous studies have provided some insight into how the MJO may change in a warming climate based on a single model or a limited number of model simulations (some of them have difficulties reproducing realistic MJO propagation). This study quantitatively examines future changes in the MJO using models from the Coupled Model Intercomparison Project

Phase 6 (CMIP6) database that realistically simulate the eastward MJO propagation. Most models project that MJO-related convection will be stronger, and the MJO will propagate faster and extend further eastward in a warming climate. The above changes are primarily due to an increase in mean moisture that peaks near the Equator over the Indo-Pacific warm pool.

1. Introduction

The Madden-Julian oscillation (MJO, Madden & Julian, 1971, 1972) is the dominant planetary-scale intraseasonal mode of climate variability in the tropics and is characterized by an eastward propagation of convection-circulation coupled system in the Indo-Pacific region with a period of approximately 30-60 days. The MJO has a strong influence on global weather and climate phenomena via teleconnections (e.g., Henderson et al. 2016; Zhang 2013) and is hence considered a major source for subseasonal-to-seasonal (S2S) predictability. Previous studies based on observational records and model simulations have shown that the MJO is projected to change substantially in a warming climate (see detailed review by Maloney et al. 2019). For example, Roxy et al. (2019) showed that the expansion of the Indo-Pacific warm pool during the twentieth and early twenty-first centuries as a result of anthropogenic warming leads to significant changes in the MJO life cycle from 1981-1999 to 2000-2018: MJO-related convective activity has changed to having a shorter duration over the Indian Ocean from an average of 19 days to 15.4 days, and longer duration over the Maritime Continent (MC) and the western Pacific from an average of 17.5 days to 23 days. In addition, several studies examined the changes in MJO precipitation and circulation using CMIP models and showed a projected increase in the amplitude of the MJO thermodynamic field (precipitation) and little change or a decrease in the amplitude of the MJO dynamic field (circulation) due to an increase in the vertical moisture gradient and static stability (e.g., Bui and Maloney 2018, 2019a, 2019b, 2020; Rushley et al. 2019). Other MJO characteristics are also projected to change in a warmer climate: eastward extension, increased propagation speed, a shorter

timescale, and more frequent MJO events than the current climate (e.g., Arnold et al. 2013, 2015; Chang et al. 2015).

Although previous studies have investigated MJO changes under anthropogenic warming scenarios, the robustness of those results is constrained by several limitations: 1) discontinuous satellite data records in the latter half of the twentieth century; 2) a limited number of model simulations being examined, i.e., the model studies are generally based on a single or only a few models; 3) oversimplified configurations in the numerical model experiments; 4) "poor" simulation of basic MJO characteristics in the older generation of models (e.g., CMIP3 and CMIP5) such as too weak an amplitude, too fast a propagation, and an exaggerated MC barrier effect (e.g., Ahn et al. 2017; Kim et al. 2014). The newly available CMIP6 database has the potential to help mitigate the above limitations, as they show significant improvement in MJO simulations compared to their older generations. There is considerably improved and coherent eastward propagation over the MC due to the reduced dry moisture bias in the mean states (Ahn et al. 2020), more realistic amplitudes of MJO precipitation and zonal winds (Orbe et al. 2020), and reduced inter-model spreads of the MJO characteristics (Chen et al. 2022).

In this study, we perform a systematic and quantitative examination of future MJO changes in a set of 23 CMIP6 model simulations that have realistic MJO propagation. Changes in MJO amplitude, propagation speed, and zonal extension and their uncertainties will be discussed with a multi-model comparison. The underlying mechanisms of the changes will be explored based on the moisture budget analysis given that the MJO propagation and maintenance are largely controlled by the physical processes that give rise to the moisture anomalies (e.g., Adames et al. 2020; Sobel and

Maloney 2013). This study provides new insights including quantitative estimates of projected future changes in various characteristics using newly developed/modified metrics, examination of model uncertainties in MJO changes in a large set of model databases, and attribution of MJO changes to mean moisture trends. This study also sets a foundation for a better understanding of how MJO impacts may change in the future.

2. Data and Method

2.1 CMIP6 Simulations and verification data

This study uses the daily output from 23 CMIP6 climate model simulations (Eyring et al. 2016; Table S1 in the supporting information) which contain a realistically simulated MJO in their historical runs. These models were selected originally from 35 CMIP6 models by applying the propagation metric defined by Ahn et al. (2020) when it is greater than 0.75. This metric was designed to indicate the robustness of MJO propagation over the MC and is calculated as the normalized 0-25-day lag-regression coefficient over MC area (100°-150°E) in models against observations. Therefore, the CMIP6 models selected in our study produce a realistic MJO propagation. The observed precipitation is derived from the Tropical Rainfall Measuring Mission 3B42 Version 7 (TRMM, Huffman et al. 2007) from 1998 to 2018. To examine future MJO projections, we use the SSP585 scenario from the ScenarioMIP runs (O'Neill et al. 2016) which follows the RCP8.5 global forcing pathway (i.e., radiative forcing of 8.5 W/m^2 by the end of the 21st century) with SSP5 socioeconomic conditions. The periods of the historical and projected future simulations are 1979-2014 and 2065-2100, respectively.

Only one ensemble member of each model (Table S1 in the supporting information) is used for a consistent comparison. Daily precipitation is used for the quantitative examination of changes in basic MJO characteristics. Specific humidity and horizontal winds derived from a subset of models (16/23) are used in the moisture budget analysis given limited data availability. All model outputs are interpolated to a horizontal grid of 2.5°×2.5° to produce consistent multimodel analyses. Anomalies are derived by first removing the first three harmonics of the annual cycle, and then applying a 25-90 day bandpass filter to extract the intraseasonal signals. The current study focuses on the boreal winter from October to March when the MJO is most active (e.g., Lu and Hsu 2017).

2.2 Moisture Budget Analysis

Following Ahn et al. (2020), an integrated moisture budget analysis between 850-700hPa is performed given that the MJO-associated moisture anomaly peaks at ~700hPa (Adames and Wallace 2015; Kiladis et al. 2005):

$$\langle\frac{\partial q}{\partial t}\rangle = -\langle u\frac{\partial q}{\partial x}\rangle - \langle v\frac{\partial q}{\partial y}\rangle - \langle\omega\frac{\partial q}{\partial p}\rangle - P + E$$

where q, u, v, and ω indicate specific humidity, zonal, meridional, and pressure velocity, respectively. P and E represent precipitation and evaporation.

3. Results

3.1 Quantitative examination of future changes in MJO characteristics

3.1.1 Propagation and spectral properties of future MJO

Hovmöller diagrams of 10°S-10°N averaged precipitation anomalies are constructed respectively for the historical and future period in each model (Figure 1), along with the TRMM precipitation. Day 0 corresponds to the day when the standard deviation of precipitation anomaly averaged over the eastern Indian Ocean (85°-95°E, 5S°-5°N) is greater than 1. The eastward MJO propagation is realistically simulated. Results of the multi-model-mean (MMM, Figures 1a-b) indicate an overall stronger MJO precipitation with an eastward extension (more discussion in the following sections).

Wavenumber–frequency power spectra of 10°S–10°N averaged un-filtered precipitation for observation and CMIP6 models are compared in Figure S1 along with their future projections. In observations, spectral peaks within the 25–100-day period at wavenumbers 1–3 are seen, consistent with previous studies (e.g., Ahn et al. 2017). Some CMIP5 models showed biases in simulating the eastward power of the MJO, which peaks at a much lower frequency/longer period (>100-day period) such as in BCC-CSM1-1, CanESM2, GFDL-ESM2M, HadGEM2-CC, HadCM3, and ACCESS1-0 (Ahn et al. 2017). This bias is still seen in some CMIP6 models, especially in ACCESS-ESM1-5, CESM2, CESM2-WACCM, EC-Earth3-Veg, HadGEM3-GC31-MM, KACE-1-0-G, MRI-ESM2-0, and NorESM2-MM. Most CMIP6 models project the future MJO to peak at a shorter period and larger spatial scale (smaller zonal wavenumber), consistent with results found in previous studies (Adames et al. 2017; Arnold et al. 2013, 2015).

3.1.2 MJO amplitude

Future changes in the MJO amplitude, propagation speed, and zonal extension are now measured in each model by quantitative metrics.

The standard deviation of the precipitation anomalies in the Hovmöller diagrams is calculated from -20 to 20 days with a longitudinal span of 30°E-160°W (green box in Figure 1a,b) as a representative of the MJO precipitation amplitude. The difference between the future and historical values normalized by the historical basis is used to measure the relative change of the MJO amplitude (Figure 2a). Most models analyzed in this study tend to project a stronger amplitude of the MJO precipitation in the future. The change is especially profound in CESM2, CESM2-WACCM, and NESM3 with an average amplitude increasing above ~30%. In contrast, some models (ACCESS-ESM1-5, BCC-CSM2-MR, CAMS-CSM1-0, and MPI-ESM1-2-LR) show a modest increase or even a decrease in the MJO precipitation. The MMM MJO precipitation amplitude is 0.71 mm/day in the current climate and will increase to 0.83 mm/day in the future, which is a ~17% increase.

Although studies generally agree that MJO precipitation amplitude will be increasing in a warmer climate (e.g., Adames et al. 2017; Bui and Maloney 2019a,b) as shown in this study, changes in MJO circulation amplitude are more uncertain. Several studies have shown stronger MJO circulations (Carlson and Caballero 2016; Pritchard and Yang 2016), while many others showed either ambiguous (Liu et al. 2013; Subramanian et al. 2014) or weakened MJO circulation intensity (Adames et al. 2017; Bui and Maloney 2018, 2019a,b; Wolding et al. 2017). Here, we revisit the amplitude change in MJO-related low-level circulation in CMIP6 models (Figure S2). The models agree with the observed patterns that low-level easterly (westerly) wind is generated to the east (west) of enhanced MJO convection. The amplitude metric defined in this study is then calculated on the filtered 850hPa zonal wind (Figure S3). The MMM suggests a ~10% increase in

low-level MJO circulation in a warmer climate which is especially profound in CESM2-WACCM. CAMS-CSM1-0, CNRM-CM6-1, CNRM-ESM2-1, EC-Earth3, FGOALS-g3, and MPI-ESM1-2-HR, on the other hand, project a decrease in MJO circulation. Future investigation is needed to examine the uncertainty of MJO circulation amplitude changes, such as how it is sensitive to the different quantification metrics of MJO circulation as we note that a contradictory result is found between this study and Wang et al. (2022). The main difference is that Wang et al. (2022) used the filtered variance of 850hPa zonal wind regardless of its dependence on MJO propagation.

3.1.3 MJO propagation extension

A metric adopted from Ahn et al. (2020) is used to measure the extension magnitude of the MJO propagation. It is calculated as the average of precipitation positive anomalies over 0-20 days, 120°-170°E in Hovmöller diagrams (dashed black box in Figure 1a). Differences between the future and historical runs normalized by the historical values are shown in Figure 2b. It is found that 19/23 (~83%) models suggest a more eastward extended MJO propagation in the future, especially in CESM2 and CESM2-WACCM. CAMS-CSM1-0, EC-Earth3-Veg, MIROC-ES2L, and NorESM2-MM, on the other hand, project a westward retreatment of the MJO propagation. The MMM of propagation extension magnitude suggests ~28% more precipitation in the easternmost reach of the MJO. The eastward extended propagation feature is further tested using the metric developed by Zhang and Ling (2017) with slight modifications such as varying reference longitudes by models. Their metric is to quantify the ending longitude of the MJO propagation calculated using the Hovmöller diagrams (e.g., Figure 1) as follows: First, draw a set of slopes that passes across the maximum precipitation center at day 0 with

different phase speeds from 3 m/s to 7 m/s with an interval of 0.1 m/s. Then, identify the longest segment along the slope that has precipitation anomaly greater than 0.5 mm/day. Lastly, compare the segment selected for each slope and find the one that has the largest averaged precipitation amplitude and the longest longitudinal distance between the starting and the endpoint. The endpoint of the selected slope is used as another propagation extension metric and the corresponding results are shown in Figure 2c to test the robustness of Figure 2b. The results are generally consistent between the two metrics (significant correlation at 0.51) that most CMIP6 simulations are projecting a more eastward extended MJO propagation except for EC-Earth3, HadGEM3-GC31-MM, MIROC-ESM2L, and NorESM2-LM. The MMM is 138.26°E for the historical run, and 143.8°E for the future run, indicating about 5° more eastward extension of the MJO precipitation in the warming climate.

3.1.4 MJO propagation speed

MJO phase speed is quantified using the phase speed of the slope that was selected in the "extension" discussion. This metric shows that MJO propagates with an average speed of 5.81 m/s in the historical runs, and 6.31 m/s in the future runs, which is ~9% increase. The relative MJO phase speed change in the individual model is shown in Figure 2d. 17/23 (~74%) models project faster MJO propagation in the warming climate. Especially in CESM2-WACCM, CNRM-CM6-1, FGOALS-g3, and MPI-ESM1-2-HR, the MJO is projected to propagate over 20% faster than that in the current climate. The MJO period is used as another metric to estimate the MJO propagation speed which is calculated from the wavenumber-frequency power spectra (Figure S1). It is the sum of the power-weighted period divided by the sum of power over the 25-100-day period for

zonal wavenumbers 1-3 (Figure 2e). In the historical runs, the MMM MJO period is 38.7 days, which decreases to 36.6 days in future runs. This ~5% shorter MJO period indicates a faster MJO propagation in the future which is consistent with the results estimated from the phase speed metric.

3.2 Plausible mechanisms based on moisture mode hypothesis

We now investigate plausible physical mechanisms associated with the future changes in MJO from a moisture mode perspective. Figures 3a-c show the Hovmöller diagrams of 10°S-10°N averaged MMM precipitation and moisture tendency anomalies associated with the historical MJO, the future MJO, and their differences. The enhanced MJO convection is tightly coupled with strong positive moisture tendency (i.e., moisture recharging) to its east which leads to eastward MJO propagation (e.g., Rushley et al. 2022). This positive moisture tendency is significantly intensified in the warming climate over 10°S-10°N, 120°E-160°W from day -5 to day 5 which has a large model agreement (not shown) and thus provides a more favorable condition for the MJO to propagate eastward. A significant correlation is found between the increased moisture recharge averaged over the above region (red boxes in Figures 3a-c) and increased MJO precipitation amplitude at 0.82. The increased moisture recharge is also significantly correlated with a more eastward MJO propagation at 0.61.

To further understand the mechanism of the intensified moisture tendency, the individual moisture budget terms are calculated by averaging over 10°S-10°N, 120°E-160°W from day -5 to day 5 where a significant change in moisture tendency is identified. The results show a dominant contribution of enhanced meridional advection to the intensified positive moisture tendency, consistent with observation (Figure S4), while

254 changes in zonal advection and the residual terms including vertical moisture advection,
255 precipitation, and evaporation play an opposite role in the moisture tendency changes.
256 The longitudinal variation of each budget term is given in Figure S4, which shows the
257 contribution of each moisture term to the total moisture tendency with respect to MJO
258 convection over the MC. In both the current and future climates, the meridional advection
259 of moisture dominates the positive moisture tendency anomaly to the east of MJO
260 convection, and the negative tendency anomaly to the west, followed by the contribution
261 from zonal advection. The cancellation effect of positive zonal advection over 110°-
262 140°E and negative zonal advection over farther east leads to the negative contribution to
263 the total moisture tendency and their change as found in Figure 3d.

264 The mean state moisture and its meridional gradient are then compared in Figure 4
265 between the historical and future runs to understand the positive change in meridional
266 moisture advection in a warming climate given that the meridional advection is
267 dominated by the advection of mean state moisture by MJO wind (e.g., Ahn et al. 2020;
268 Kang et al. 2021). The results indicate a significant increase in the mean moisture in a
269 warming climate with the largest magnitude near the Equator. This pattern leads to a
270 steepening of the meridional gradient of mean moisture in the tropics, especially over the
271 Indo-Pacific warm pool and eastern Pacific and hence a stronger meridional advection of
272 moisture. The above processes favor stronger moisture recharging to the east of enhanced
273 MJO convection assuming the MJO wind remains unchanged, leading to the more
274 eastward extension of MJO in the warming climate (Figures 1 and 2). In addition to its
275 impacts on MJO extension, the steepening of the meridional moisture gradient also
276 positively contributes to the faster MJO phase speed with a correlation between increased

277 moisture tendency and increased phase speed at 0.49. This is consistent with the
278 relationship that MJO phase speed is proportional to the meridional gradient of mean
279 moisture (Adames and Kim 2016). The intensification of MJO precipitation amplitude,
280 on the other hand, has been documented to be largely attributed to the increased vertical
281 moisture gradient in the lower troposphere in response to surface warming (e.g., Wolding
282 et al. 2017) and is verified by this study (not shown).
283

284 4. Summary and Discussion

285 This study quantitatively examines the future changes in MJO and their mechanisms in
286 23 CMIP6 models. In general, the multi-model mean projects a ~17% increase in MJO
287 precipitation amplitude (model ranges from -10% to 70%), ~10% increase in MJO
288 circulation amplitude (ranges from -20% to 80%), ~9% increase in propagation speed
289 (ranges from -30% to 40%), ~2 days shorter period (ranges from 5-day decrease to 2-day
290 increase), and ~5° eastward extension (ranges from 20° westward retreatment to 20°
291 eastward extension). The more eastward extension and faster phase speed may be
292 attributed to the steepening of the meridional gradient of mean moisture over the Indo-
293 Pacific warm pool in a warming climate that leads to stronger moisture recharging during
294 the MJO propagation.
295 This study uses a variety of metrics for quantifying the future changes in MJO
296 propagation and phase speed and their uncertainty. The results showed that models
297 generally have large consistency in projecting future MJO changes and the uncertainty
298 mainly arises from the different metrics being used to quantify the changes. For example,
299 in FGOALS-g3 and MPI-ESM1-2-LR, the MJO propagation speed is faster in the future

climate, yet the MJO period is longer, suggesting an opposite projection of MJO phase speed by different metrics. The different propagation extension metrics also show different projections in EC-Earth3-Veg and NorESM2-LM/MM. The causes of the uncertainty of future MJO changes merit further investigation. It is also important to examine how sensitive the projected MJO is to the model projection of the mean state changes. This is motivated by the studies showing that MJO projections are largely dependent on the projected sea surface temperature patterns (e.g., Maloney and Xie 2013; Takahashi et al. 2011).

Here, we diagnosed future projected changes in the MJO to help lay a foundation for a more detailed assessment of S2S predictability in our changing climate. Studies have shown that the MJO significantly modulates precipitation extremes in many regions around the globe including Indonesia, the western Pacific, Brazil, and the Western U.S. (e.g., Jones et al. 2004; Muhammad et al. 2021; Vasconcelos et al. 2018; Wang et al. 2023). Zhou et al. (2020) indicated that the most eastward extended MJO and its teleconnections would lead to larger impacts on precipitation over California in the future climate. How MJO-associated precipitation extremes may change in the future as a result of the MJO and mean state changes will be examined in our future study.

Data Availability Statement

The CMIP6 models used in the study are listed in Supporting Information. Their outputs were downloaded from the CMIP archive at https://esgf-node.llnl.gov/projects/esgf-llnl. The ERA5 reanalysis is available at https://doi.org/10.24381/cds.bd0915c6. The TRMM precipitation data can be obtained from https://disc.gsfc.nasa.gov/datasets/TRMM_3B42_Daily_7/summary.

Acknowledgements

This research was supported by the California Department of Water Resources Atmosphere River Program Phase III (contract number 4600014294). H. Kim was supported by U.S. NSF grant AGS-1652289, NOAA grant NA22OAR4590168 and NA22OAR4590216, and Korean Meteorological Administration Research and Development Program under Grant KMI2021-01210. K. Guirguis and A. Gershunov were supported by the U.S. Department of the Interior via the Bureau of Reclamation (USBR - R15AC00003), California Department of Water Resources (4600010378 UCOP2 - 11), and NOAA's California and Nevada Applications Program award NA11OAR43101.

References

Adames, Á. F., and J. M. Wallace, 2015: Three-dimensional structure and evolution of the moisture field in the MJO. *J. Atmos. Sci.*, **72,** 3733-3754.

Adames, Á. F., and D. Kim, 2016: The MJO as a dispersive, convectively coupled moisture wave: Theory and observations. *J. Atmos. Sci.*, **73**, 913–941.

Adames, Á. F., D. Kim, A. H. Sobel, A. Del Genio, and J. Wu, 2017: Characterization of moist processes associated with changes in the propagation of the MJO with increasing CO2. *J. Adv. Model. Earth Syst.*, **9,** 2946-2967.

Adames, Á. F., D. Kim, E. D. Maloney, and A. H. Sobel, 2020: The moisture mode framework of the Madden–Julian oscillation. *The Multiscale Global Monsoon System*, World Scientific, 273-287.

Ahn, M.-S., and Coauthors, 2017: MJO simulation in CMIP5 climate models: MJO skill metrics and process-oriented diagnosis. *Clim. Dyn.*, **49,** 4023-4045.

Ahn, M.-S., and Coauthors, 2020: MJO propagation across the Maritime Continent: Are CMIP6 models better than CMIP5 models? *Geophys. Res. Lett.*, **47,** e2020GL087250.

Arnold, N. P., Z. Kuang, and E. Tziperman, 2013: Enhanced MJO-like variability at high SST. *J. Climate*, **26,** 988-1001.

Arnold, N. P., M. Branson, Z. Kuang, D. A. Randall, and E. Tziperman, 2015: MJO intensification with warming in the superparameterized CESM. *J. Climate*, **28,** 2706-2724.

Bui, H. X., and E. D. Maloney, 2018: Changes in Madden-Julian Oscillation precipitation and wind variance under global warming. *Geophys. Res. Lett.*, **45**, 7148-7155.

Bui, H. X., and E. D. Maloney, 2019a: Mechanisms for global warming impacts on Madden-Julian Oscillation precipitation amplitude. *J. Climate*, **32**, 6961-6975.

Bui, H. X., and E. D. Maloney, 2019b: Transient response of MJO precipitation and circulation to greenhouse gas forcing. *Geophys. Res. Lett.*, **46,** 13546-13555.

Bui, H. X., and E. D. Maloney, 2020: Changes to the Madden-Julian Oscillation in coupled and uncoupled aquaplanet simulations with 4xCO2. *J. Adv. Model. Earth Syst.*, **12,** e2020MS002179.

Carlson, H., and R. Caballero, 2016: Enhanced MJO and transition to superrotation in warm climates. *J. Adv. Model. Earth Syst.*, **8,** 304-318.

Chang, C. W. J., W. L. Tseng, H. H. Hsu, N. Keenlyside, and B. J. Tsuang, 2015: The Madden-Julian Oscillation in a warmer world. *Geophys. Res. Lett.*, **42,** 6034-6042.

Chen, G., J. Ling, R. Zhang, Z. Xiao, and C. Li, 2022: The MJO from CMIP5 to CMIP6: Perspectives from tracking MJO precipitation. *Geophys. Res. Lett.*, **49,** e2021GL095241.

Eyring, V., S. Bony, G. A. Meehl, C. A. Senior, B. Stevens, R. J. Stouffer, and K. E. Taylor, 2016: Overview of the Coupled Model Intercomparison Project Phase 6 (CMIP6) experimental design and organization. *Geosci. Model Dev.*, **9,** 1937-1958.

Henderson, S. A., E. D. Maloney, and E. A. Barnes, 2016: The influence of the Madden–Julian oscillation on Northern Hemisphere winter blocking. *J. Climate*, **29**, 4597–4616, doi:10.1175/JCLI-D-15-0502.1.

Huffman, G. J., and Coauthors, 2007: The TRMM multisatellite precipitation analysis (TMPA): Quasi-global, multiyear, combined-sensor precipitation estimates at fine scales. *J. Hydrometeorol.*, **8,** 38-55.

Jones, C., D. E. Waliser, K. Lau, and W. Stern, 2004: Global occurrences of extreme precipitation and the Madden–Julian oscillation: Observations and predictability. *J. Climate*, **17**, 4575–4589.

Kang, D., D. Kim, M.-S. Ahn, and S.-I. An, 2021: The role of the background meridional moisture gradient on the propagation of the MJO over the maritime continent. *J. Climate*, **34,** 6565-6581.

Kiladis, G. N., K. H. Straub, and P. T. Haertel, 2005: Zonal and vertical structure of the Madden–Julian oscillation. *J. Atmos. Sci.*, **62,** 2790-2809.

Kim, D., and Coauthors, 2014: Process-oriented MJO simulation diagnostic: Moisture sensitivity of simulated convection. *J. Climate*, **27,** 5379-5395.

Liu, P., and Coauthors, 2013: MJO change with A1B global warming estimated by the 40-km ECHAM5. *Climate Dyn.*,**41,** 1009-1023.

Lu, W., and P.-C. Hsu, 2017: Factors controlling the seasonality of the Madden-Julian Oscillation. *Dyn. Atmospheres Oceans*, **78,** 106-120.

Madden, R. A., and P. Julian, 1971: Detection of a 40–50 day oscillation in the zonal wind in the tropical Pacific. *J. Atmos. Sci.*, **28**, 702–708, doi:10.1175/1520-0469(1971)028,0702:DOADOI.2.0.CO;2.

Madden, R. A., and P. Julian, 1972: Description of a global-scale circulation cells in the tropics with a 40–50 day period. *J. Atmos. Sci.*, **29**, 1109–1123, doi:10.1175/1520-0469(1972)029,1109:DOGSCC.2.0.CO;2.

Maloney, E. D., Á. F. Adames, and H. X. Bui, 2019: Madden–Julian oscillation changes under anthropogenic warming. *Nat. Clim. Change*, **9,** 26-33.

Maloney, E. D., and S. P. Xie, 2013: Sensitivity of tropical intraseasonal variability to the pattern of climate warming. *J. Adv. Model. Earth Syst.*, **5,** 32-47.

Muhammad, F. R., S. W. Lubis, and S. Setiawan, 2021: Impacts of the Madden–Julian oscillation on precipitation extremes in Indonesia. *Int. J. Climatol.*, **41**, 1970–1984.

O'Neill, B. C., and Coauthors, 2016: The scenario model intercomparison project (ScenarioMIP) for CMIP6. *Geosci. Model Dev.*, **9,** 3461-3482.

Orbe, C., and Coauthors, 2020: Representation of modes of variability in six US climate models. *J. Climate*, **33,** 7591-7617.

Pritchard, M. S., and D. Yang, 2016: Response of the superparameterized Madden–Julian oscillation to extreme climate and basic-state variation challenges a moisture mode view. *J. Climate*, **29,** 4995-5008.

Roxy, M., P. Dasgupta, M. J. McPhaden, T. Suematsu, C. Zhang, and D. Kim, 2019: Twofold expansion of the Indo-Pacific warm pool warps the MJO life cycle. *Nature*, **575,** 647-651.

Rushley, S. S., D. Kim, and Á. F. Adames, 2019: Changes in the MJO under greenhouse gas–induced warming in CMIP5 models. *J. Climate*, **32,** 803-821.

Sobel, A., and E. Maloney, 2013: Moisture modes and the eastward propagation of the MJO. *J. Atmos. Sci.*, **70,** 187-192.

Subramanian, A., M. Jochum, A. J. Miller, R. Neale, H. Seo, D. Waliser, and R. Murtugudde, 2014: The MJO and global warming: A study in CCSM4. *Climate Dyn.*, **42,** 2019-2031.

Takahashi, C., N. Sato, A. Seiki, K. Yoneyama, and R. Shirooka, 2011: Projected future change of MJO and its extratropical teleconnection in East Asia during the northern winter simulated in IPCC AR4 models. *Sola*, **7,** 201-204.

Vasconcelos, F. C., Jr., C. Jones, and A. W. Gandu, 2018: Interannual and intraseasonal variations of the onset and demise of the pre-wet season and the wet season in the northern Northeast Brazil. *Rev. Bras. Meteor.*, **33**, 472–484.

Wang, J., H. Kim, and M. J. DeFlorio, 2022: Future changes of PNA-like MJO teleconnections in CMIP6 models: Underlying mechanisms and uncertainty. *J. Climate*, **35,** 3459-3478.

Wang, J., M. J. DeFlorio, B. Guan, and C. M. Castellano, 2023: Seasonality of MJO Impacts on Precipitation Extremes over the Western United States. *J. Hydrometeorol.*, **24,** 151-166.

Wolding, B. O., E. D. Maloney, S. Henderson, and M. Branson, 2017: Climate change and the M adden-J ulian O scillation: A vertically resolved weak temperature gradient analysis. *J. Adv. Model. Earth Syst.*, **9,** 307-331.

Zhang, C., 2013: Madden–Julian oscillation: Bridging weather and climate. *Bull. Amer. Meteor. Soc.*, **94**, 1849–1870, doi:10.1175/BAMS-D-12-00026.1.

Zhang, C., and J. Ling, 2017: Barrier effect of the Indo-Pacific Maritime Continent on the MJO: Perspectives from tracking MJO precipitation. *J. Climate*, **30,** 3439-3459.

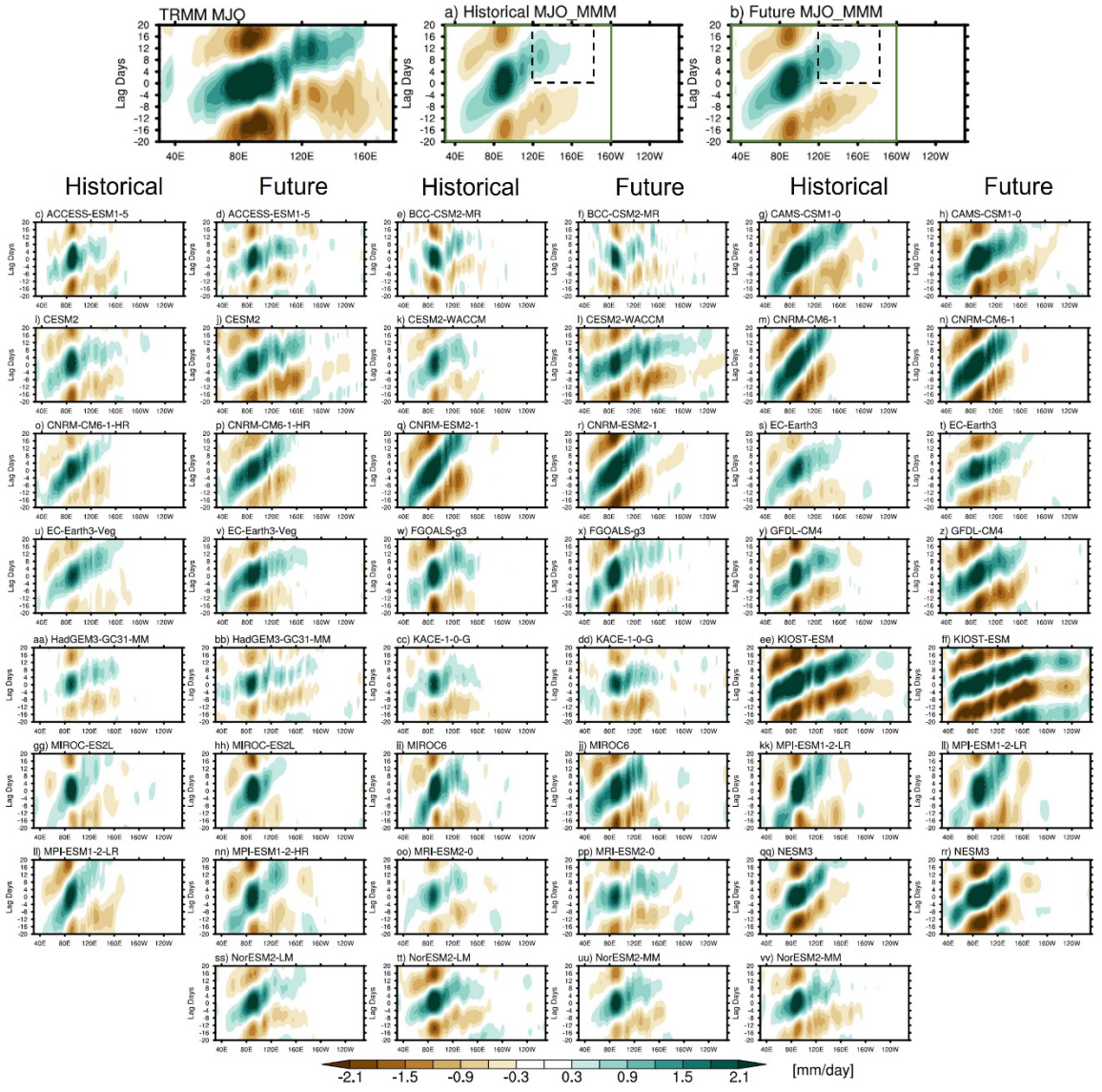

FIG. 1. Lag-longitude diagram of 10°S-10°N averaged 25-90-day filtered precipitation anomalies for TRMM, MMM (a) historical and (b) future MJO based on time series averaged over 85°-95°E, 5°S-5°N greater than one standard deviation. (c)-(vv) are similar to (a) and (b) except for historical and future MJO in individual CMIP6 models. The green box (30°E-160°W, -20 to 20 days) in (a) and (b) shows the region used for calculating the MJO amplitude metric. The black dashed box

453 (120°-170°E, 0-20 days) in (a) and (b) indicates the region used for calculating
454 the MJO propagation extension metric.
455

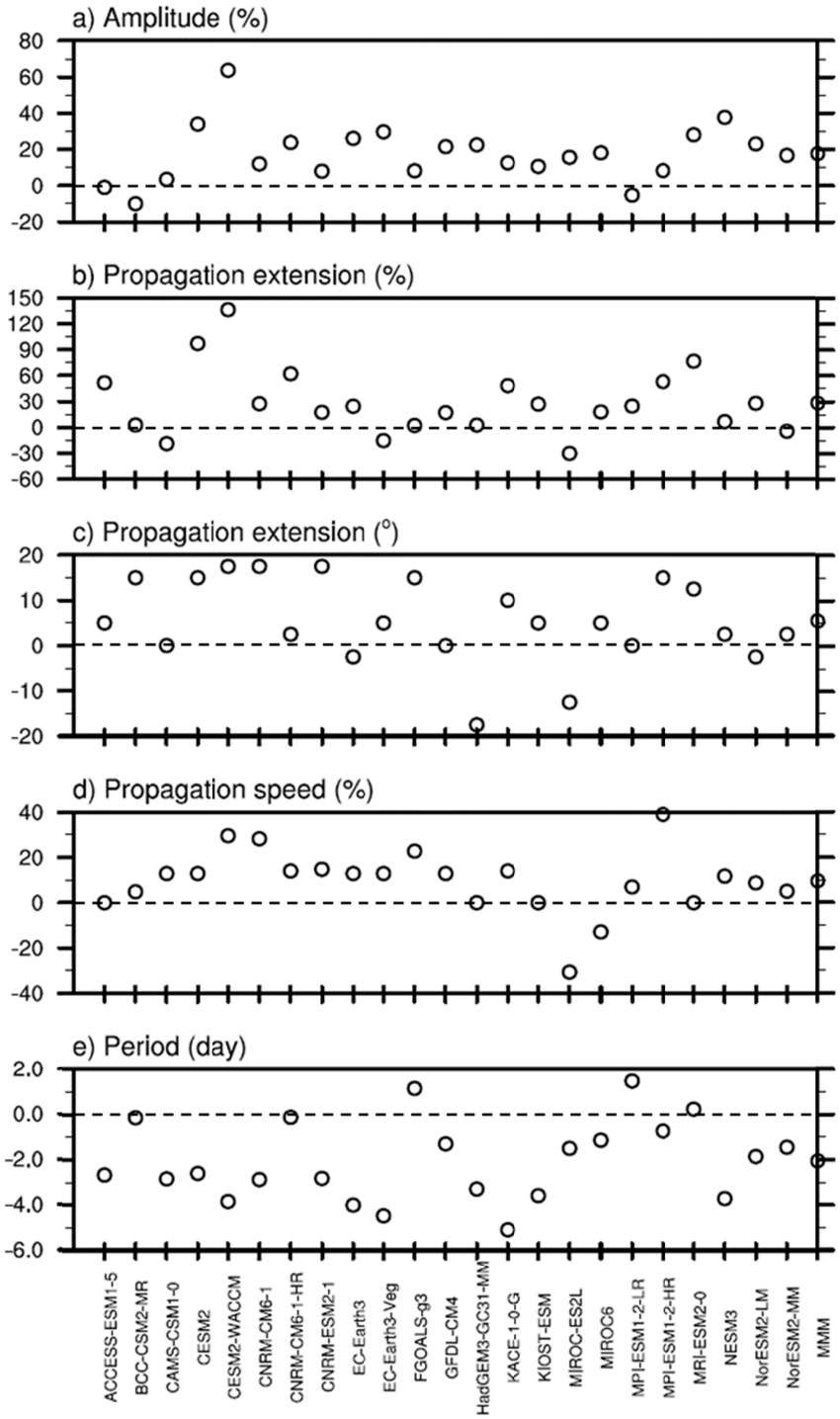

457

460 FIG. 2. Future changes in (a) MJO precipitation amplitude, (b)-(c) propagation extension,
461 (d) propagation speed, and (e) period projected by each model and the MMM
462 (open circles).

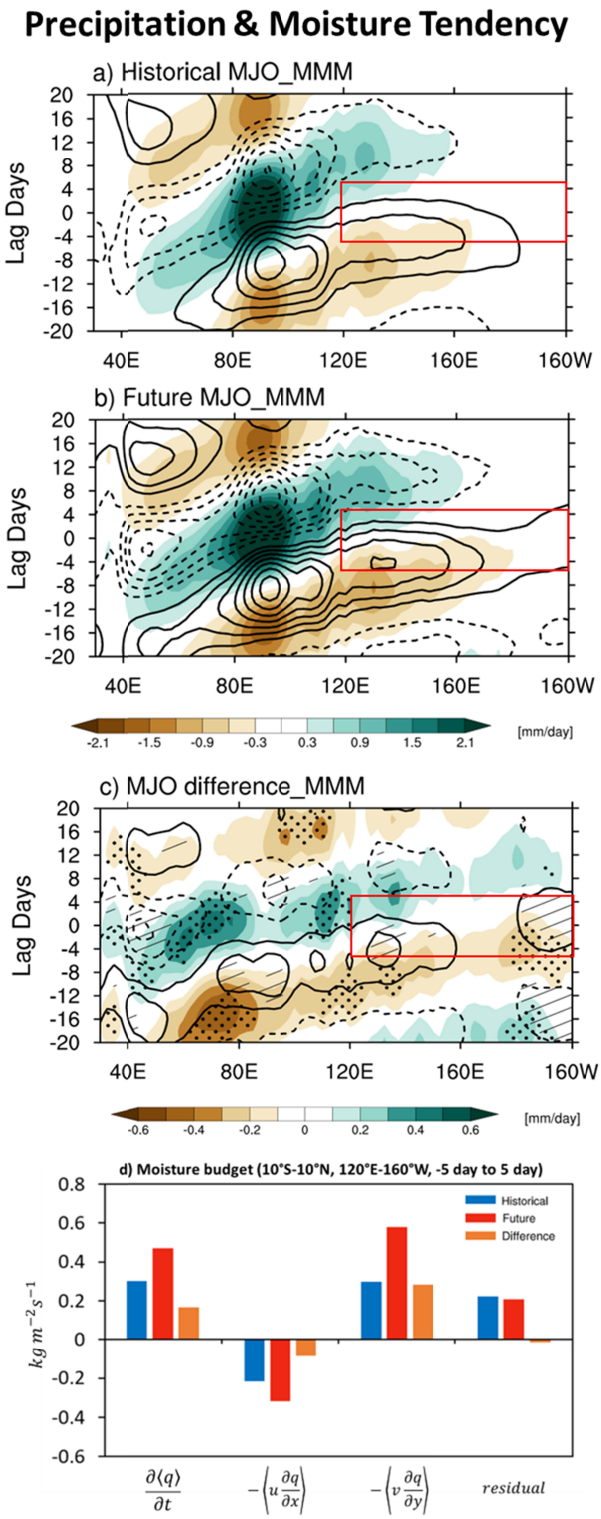

FIG. 3. (a)-(b) Same as Figure 1, but for MMM filtered precipitation anomalies (shading) and 850-700hPa vertically integrated moisture tendency anomalies (contour,

463 $0.3 \times 10^{-6} kgm^{-2}s^{-1}$ interval) in historical and future climates, respectively. (c)
464 Difference between (b) and (a), which represents the future change in MJO
465 precipitation (shading) and moisture tendency (contour, $0.2 \times 10^{-6} kgm^{-2}s^{-1}$
466 interval). Dots and hatch in (c) denote the significant difference in precipitation
467 and moisture tendency, respectively, at the 0.05 significance level. The red box in
468 each plot denotes the region (120°E-160°W, -5 to 5 days) where the calculation of
469 contribution from each moisture budget term is conducted. (d) 850-700hPa
470 integrated moisture budget (unit: $10^{-6} kgm^{-2}s^{-1}$) averaged over the red box in
471 (a)-(c) where the change in moisture tendency is significant.
472

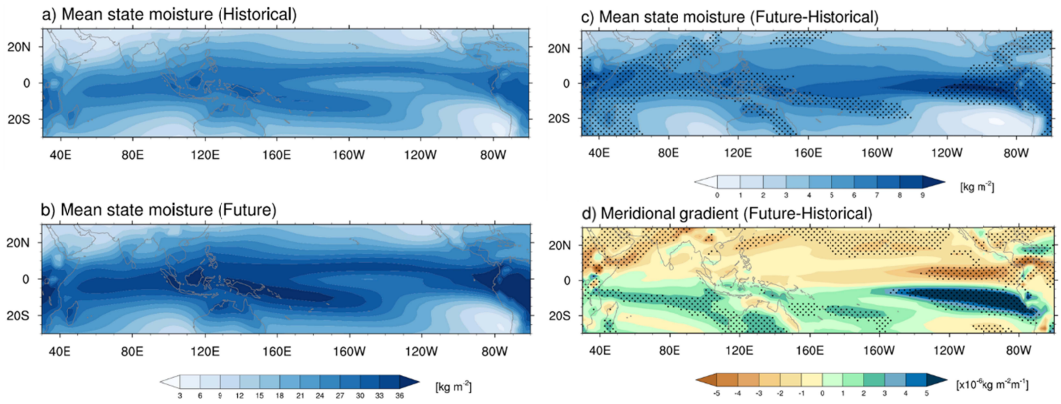

474

477 FIG. 4. (a) Historical and (b) future 850-700hPa integrated mean state moisture and (c)
478 their difference. (d) Future changes in meridional gradient of mean moisture. Dots
479 in (c) and (d) indicate the difference at the 0.05 significance level.